The impact of ion drift in a Transcutaneous Electrical Stimulation model
Biomedical Engineering: Master Thesis

Keywords: TES, neuron activation, ion drift, conductivity, COMSOL, FEM

LUND
UNIVERSITY

Faculty of engineering LTH
Department of Biomedical Engineering

Erik Blåe, Oscar Tuvesson

September 26, 2022

Supervisor:
Nebojsa Malesevic
Examiner:
Christan Antfolk

1 Abstract

A major area of research in neuroscience is the effect of stimulating nerves into activation from extrinsic stimuli. This is commonly done with electric currents and external skin-contact electrodes. Research has shown that this method is efficient for producing muscle activation and that different current waveforms produce differing levels of activation and discomfort. This report aims to augment existing transcutaneous electric stimulation models with the effects of ion drift in the electric field caused by the electrodes and investigate how it affects nerve activation. This was done by creating a representative FEM model of the human forearm and directly simulating the effects of introducing ion drift into the model. Models for ionic effects on both electrical conductivity and charge density were included. Simulations showed a very limited effect on nerve activation and that the contributions from changes in ion concentration due to drift was small. Thereafter a 2D-axis symmetric model with the more accurate and costly Nernst Planck Poisson equations showed that the size of charge accumulation and its screening effect on the potential field were both small. Lastly it was studied wether the augmented model could account for different current waveforms yielding different nerve activation patterns, however this could not be replicated. The conclusion from this work is thus that ion drift on the macroscopic scale as modelled here only gives small, almost non-significant results.

Contents

2 Introduction

2.1 Preface

This master thesis have been intensely worked on in the months of June, July, August and September 2022. This report has been produced through the Biomedical Engineering institution at LTH. The examinator of the report is Christian Antfolk and the supervisor is Nebojsa Malesevic. We would like to thank them for finding this interesting subject for us to research and for the pleasure of working with them, as well as for them always being quick to answer emails and to book meetings.

2.2 Problem formulation

The project is built around the exploration of three major questions:

- Is it possible to augment the existing transcutaneous electrical stimulation (TES) model for predicting nerve activation with ion diffusion and drift?
- Can the eventual effects of ion diffusion, be manipulated to alter nerve activation?
- What is the next step in order to further mimic reality within this subject?

2.3 Limitations

- Extracellular ion concentration only affects bulk conductivity and electrostatic charge density, effects on action potential is not taken into account
- Only axial nerve bundles are modelled, in a regular body nerve bundles go in many directions.
- The arm was modelled as pure fluid with decreased ion mobility. This matches the electrical conductivity properties but slightly overestimated the charge density.
- Electrostatic ion-ion-interactions are not included in the nominal model.

- Finite element analysis (FEM) mesh resolution is limited by use of consumer computing hardware.

3 Background

3.1 Neuromuscular system

In order to grasp this rapport it is essential to have a basic understanding how muscles are innervated and how signals are transmitted in the central nervous system (CNS). Therefore this section of the report is going to cover how action potentials in neurons are generated, what a motor unit and motor pool is and how an action potential is propagated throughout the axons.

Neuron

A neuron transmits signals from and to the brain. In the central nervous system there are afferent and efferent neurons. Efferent nerves run from the CNS out to the muscles. An afferent nerve go in the opposite direction, from a muscle. The neuron has a unique anatomy which is fine tuned for functionality. Figure 1 shows a neuron. A signal is recieved through the dendrites or on the soma, and is then propagated forward through the axon hillock into the axon via electrochemical mechanisms. The axon is a tail like structure which is surrounded by a thick, fatty substance called myelin. Myelin increases the neurons ability to transmit a signal. Along the axon there exists intervals without myelin called Ranviers nodes which are packed with different ion channels that have a functionality in amplifying signals. Note that different neurons have a different amount of myelinesation which give different propagation speeds dependent on the neuron type. Lastly the axon branches out in different terminals and presynaptic clefts which hold different neurotransmitters.

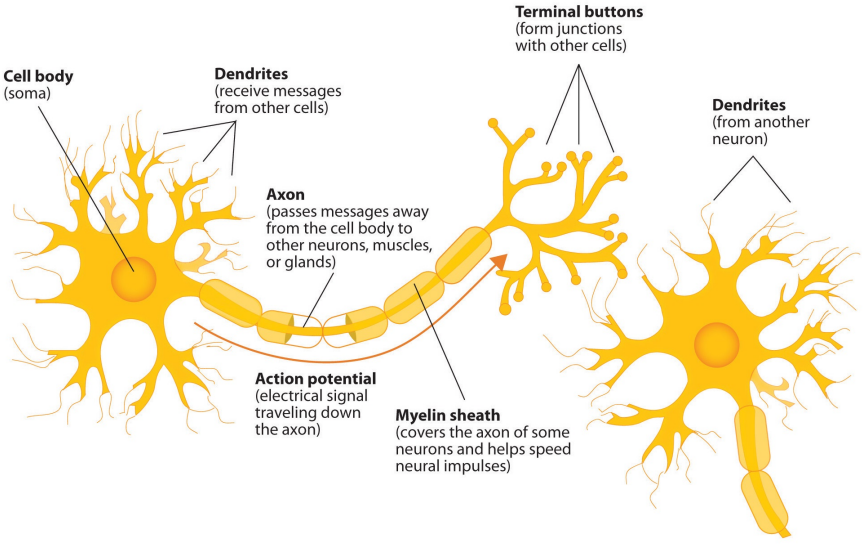

Figure 1: A neuron. Figure taken from [1] (Non-Commercial use permitted).

A motor unit is the combination of a motor neuron (efferent neuron which interacts with a muscle fiber) and all skeleton muscle fibers it innervates. A muscle comprises a number of motor units which create a motor pool. A muscle contraction occurs when a motor neuron receives an action potential where it then releases neurotransmitters from the synapse which acts on the muscle fibers which in turn gives rise to chemical effects inside the muscle fiber. A motor unit is visualized in the following figure:

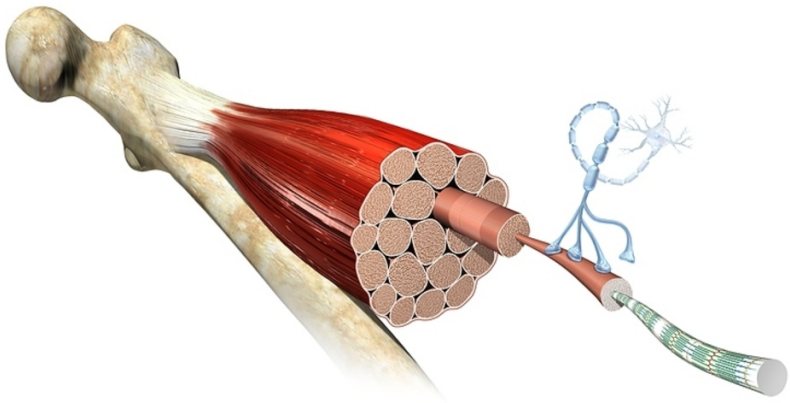

Figure 2: Motor unit. Figure taken from [2].

In order for a neuron to produce a signal it needs to be provided with an electrical action potential. A neuron has a rest potential at around -70 mV as a consequence of its semi-permeable membrane and different active pumps which keeps up an ion concentration. If given an external effect, be it through gap junctions or neurotransmitters or an external voltage field, the membrane potential can begin a depolarisation. In the membrane there exists voltage regulated sodium channels, if the depolarisation is big enough these will activate and open and a depolarisation spike will be given. This is the electrochemical event required to create a signal transmission. Thereafter potassium channels will open and the sodium channels will close, causing a hyperpolarisation (an undershoot of the rest potential) which is eventually restored by active pumps [3]. This process, an action potential, as described is seen in the underlying figure:

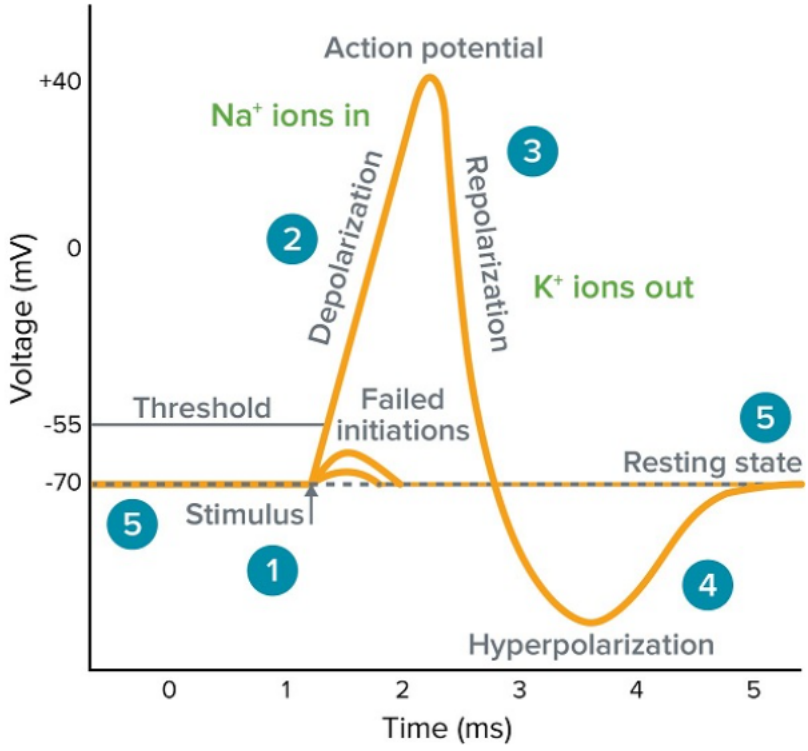

Figure 3: Action potential curve. Figure taken from [3] (Non-Commercial use permitted).

It is possible with a noninvasive power source to give rise to action potentials in neurons. This is done by placing electrodes on the skin surface, preferably at so called motor points which are spots on the human exterior that has minimal depth to neuron bundles. The power source can thus alter the extracellular potential around a cell and create a depolarisation which lead to an action potential for the neuron [3].

3.2 TES model

In recent years a large area of research has been modelling of neuron activation. Several systematic studies were made in the Kuhn thesis, thereafter

the Frontiers paper used today's existing models and presented two different more detailed modelling approaches [3][4]. In this section a number of important findings will be presented in order to provide background to this report.

The Kuhn thesis set out to create a transient electrical stimulation model (TES) by combining a transient finite element model with a neuron activation model to describe nerve activation. With the help of this model they thereafter examined which parameters influenced nerve activation the most and if inhomogeneities (such as arteries and sweat pores etc) as well as more realistic arm geometries affect neuron activation.

Geometrical models

Kuhn et al [3] examined if a realistic arm geometry (taken from MRI scans) and modelling of small scale inhomogeneities was required to make accurate predictions, but it was found that an approximative cylindrical arm geometry with no inhomogeneities yielded comparably results. The representative geometries is illustrated in figure 4 while the parameters and values which represents each layer in the arm are given in table 1. Kuhn et al [3] in section 6.7.3 examined exactly this and found that the cylinder is sufficient with at most 2.9 % difference. Therefore they reached the conclusion that a cylindrical geometry gives sufficiently reliable results to justify not using the realistic geometry, which allows for faster and more efficient modelling [3].

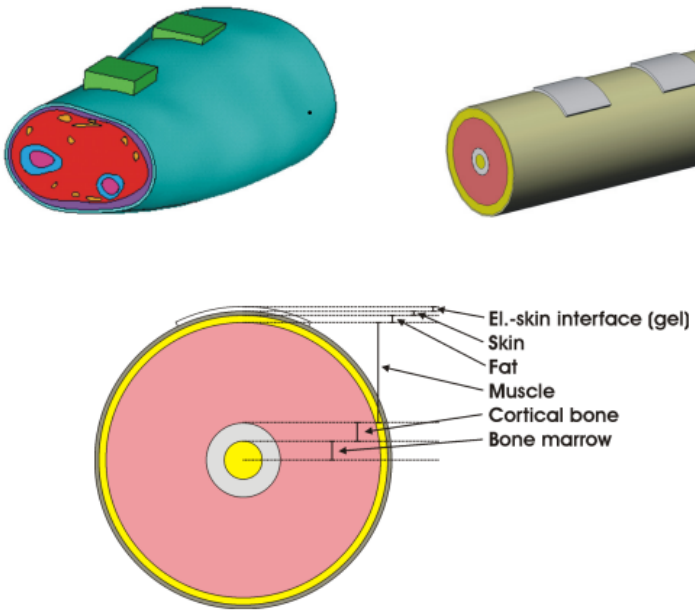

Figure 4: Geometric constellations in Kuhn article, top left is described by MRI scanned arm while top right and bottom describe the cylindrical geometry. Figure taken from [3] (Non-Commercial use permitted).

Material	Standard width [mm]	ρ [Ωm]	ϵ_r
Electrode interface	1	300	1
Skin	1.5	700	6000
Fat	2.5	33	25000
Muscle (axial)	33.5	3	120000
Muscle (radial)	33.5	9	40000
Cortical bone	6	50	3000
Bone marrow	6.5	12.5	10000

Table 1: Standard width, resistivity and relative permittivity for different tissues as implemented in Kuhn et al [3]. Note, the standard deviation for different tissues are not seen in this table.

Theory of charge accumulation

When charge accumulates under an electrode, potential screening is bound to occur. This happens because when a current flows from the positive electrode to ground the charge carrying ions cannot pass through the skin into the electrode, resulting in an accumulation of positive ions at the ground electrode and negative ions at the positive electrode. Under constant current electrode conditions this will eventually mean that higher voltage is needed to run the same current due to the potential being effectively reduced by screening [5]. The physical reason for the potential screening is that the ion accumulation layer creates its own electrostatic potential field which partially "cancels" out the produced field of the electrodes.

Effects of different waveform shapes

Recent empirical studies have shown that the current stimuli shape has an effect on the comfort of patients, amount of motor neurons stimulated, as well as on neuron targeting precision [6] [7]. However as of yet a framework for how this happens on a biological level has not been derived.

Hybrid FEM/cable-equation approach

COMSOL Multiphysics Simulation Software is a licensed software created for FEM simulations and user friendliness which offers a wide range of physics modules [8]. Sebastien Joucla et al. presented two major ways to model extracellular electrical neural stimulation [4]. In this report one of these for modelling in COMSOL will be shortly summarized as a workflow.

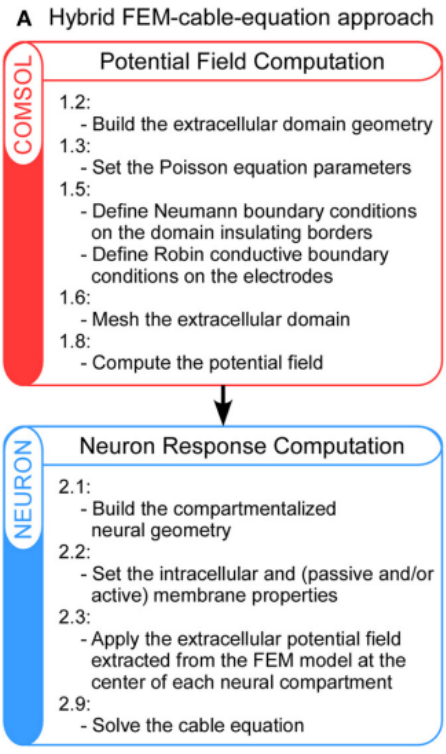

Figure 5: Workflow for a FEM-cable equation approach. Figure taken from [4].

The figure above describes the workflow in COMSOL. Build an extracellular geometry, set equation parameters, define all the boundary conditions and mesh the extracellular domain. Thereafter COMSOL computes the potential field after which it is possible to extract the element voltage in order to solve a cable equations for neuron activation in another program, which in the article is the program suite NEURON. For completeness the COMSOL solver will be shortly presented.

To understand COMSOL solvers three problem cases are presented: a linear static/transient problem, a static non linear problem, and a transient non linear problem. For linear problems every physics module has a default solver in COMSOL which quickly and accurately solves the problem [9].

For static nonlinear problems COMSOL use the standard Newton Raphson solver which includes a non physical damping factor which the user can alter for stability [10]. Lastly, the most complicated problem, a transient non linear problem can be solved in COMSOL with three different type of solvers: Backward Differentiation Formula (BDF), Generalized alpha, and Runge-Kutta Methods. These are good for stiff (numerically unstable) transient problems, however these problems are sensitive to mesh resolution and time step size and will fail to converge unless these parameters are chosen with care. Therefore the user gets freedom to alter things like time step size, mesh, relative tolerance and much more in order to solve and obtain convergence [11].

4 Mathematical models

This section will go through the conventional model of electrodynamics used in previous work and its underlying physics, the physics of ions and their dynamics, and finally augment the conventional model with the physics of ion flow.

4.1 Fundamental electrodynamics

The mathematical basis for modelling the electrodynamics of human tissue are the Maxwell's equations:

$$\begin{cases} \nabla \times H = J + \frac{\partial D}{\partial t} \\ \nabla \times E = -\frac{\partial B}{\partial t} \\ \nabla \cdot B = 0 \\ \nabla \cdot D = \rho \end{cases} \tag{1}$$

, where H is the magnetic field strength, B is the magnetic flux density, J is the current density, E is the electric field, D is the electric displacement field, and ρ is the electric charge density.

As in previous work the assumption is made that the magnetic fluxes involved are small (due to lack of inductors and the relatively low frequencies involved), and that the E-field curl is trivially small. This allows for the introduction of an electric scalar potential field V which simplifies the model considerably [12]:

$$-\frac{\partial B}{\partial t} = 0 \quad \Longrightarrow \quad E = -\nabla V \tag{2}$$

The relationships between the electric field E, the displacement field D, and

the current density J is given by:

$$\begin{cases} \mathrm{D} = \epsilon E \\ \mathrm{J} = \sigma E \end{cases} \tag{3}$$

, where σ is the material conductivity and ϵ is the material permittivity. Under these conditions the equation for magnetic field strength curl becomes:

$$\nabla \times H = -\sigma \nabla V + \frac{\partial}{\partial t} D \tag{4}$$

Combining this with the the curl divergence identity ($\nabla \cdot [\nabla \times A] = 0$ for any field A) and operator linearity yields the following divergence equation:

$$\nabla \cdot (\sigma \nabla V) = \frac{\partial}{\partial t} (\nabla \cdot D) \tag{5}$$

This is the sought after partial differential equation (PDE) that can be used to solve for the potential field, and it can be written on two forms:

$$\nabla \cdot (\sigma \nabla V + \epsilon \nabla [\frac{\partial}{\partial t} V]) = 0 \quad or \quad \nabla \cdot (\sigma \nabla V) = \frac{\partial}{\partial t} \rho \tag{6}$$

Where the latter form contains the useful term ρ linking the potential field directly to the space charge density.

4.2 The classical volume conductor

Human tissue is both inhomogenous on the cellular scale and anisotropic on the macroscopic scale [3]; On the cellular level the tissue cannot be treated as a smooth solid, and on the macroscopic scale the material properties are direction dependent. Furthermore charge is carried by solvated ions rather than conductance-band electrons, leading to a concentration-dependent conductivity which complicates modelling.

In previous work [3] it was established that the non-homogenous nature of the tissue can be averaged out and ignored, resulting in a classical rank-2 conductivity tensor on the form:

$$\boldsymbol{\sigma} = \begin{bmatrix} \sigma_{11} & \sigma_{12} & \sigma_{13} \\ \sigma_{21} & \sigma_{22} & \sigma_{23} \\ \sigma_{31} & \sigma_{32} & \sigma_{33} \end{bmatrix} \tag{7}$$

Experiments have shown [3] all tissues except muscle tissue was found to be sufficiently isotropic except muscle tissue, which was found to be orthotropic with respect to the muscle fiber direction. In the first case the conductivity tensor is reduced to:

$$\boldsymbol{\sigma} = \sigma_0 I \tag{8}$$

where I is the identity matrix, and in the latter case the the tensor reduces to:

$$\boldsymbol{\sigma} = \begin{bmatrix} \sigma_{11} & 0 & 0 \\ 0 & \sigma_{22} & 0 \\ 0 & 0 & \sigma_{33} \end{bmatrix} \tag{9}$$

, with σ_{11} being the conductivity in the direction of the muscle fibers and $\sigma_{22} = \sigma_{33}$ is the conductivity orthogonal to the fibers.

This conductivity model forms basis of the volume conductor used in the Kuhn article. It does not model any ions or space charges in the conductor model, and thus uses a reduced form of equation 6:

$$\nabla \cdot (\sigma \nabla V) = 0 \tag{10}$$

, which is time invariant. Later in this chapter (6.7) it will be explained in detail how the second spatial derivative of the potential along the nerve is the determining factor for nerve activation. The time invariant voltage-current relation given above causes the second derivative to also become time invariant, which in turn implies that all current wave forms should have the same potential second derivative for any given electrode voltage. This phenomenon is why the conventional volume conductor model cannot account for the different effects of different wave forms.

4.3 Ion distribution and flux

Ion drift in a bulk solution is in the literature [13][14] described by the Nernst Planck equations. To model the dynamics of solvated ions in the electric field the volume-conductor-model of previous work has to be appended. To this end the Nernst-Planck equations could thus be chosen to model the concentration of ion species c_s:

$$\begin{cases} \frac{\partial}{\partial t} c_s + \nabla \cdot J_s = 0 \\ J_s = -D\nabla c_s + c_s v - \frac{Dze}{k_b T} c_s E \end{cases} \tag{11}$$

, where c_s is species concentration, J_s is the concentration flux, D is diffusivity, v is the advection velocity vector, z is species charge, e is the elementary charge, and E is the electric field vector.

No bulk flow of fluid will be included in the model, and thus the advection vector is zero:

$$J_s = -D\nabla c_s - \frac{Dze}{k_b T} c_s E \tag{12}$$

The distribution of the ionic species create a charge distribution in the solution, which is given by the concentration as:

$$\rho(c_1, c_2, ...c_N) = \sum_{k=1}^{N} c_k e N_A \tag{13}$$

, where N_A is Avogadro's constant. The tissue is overall electrically neutral, introducing the condition that [15]:

$$\oiiint_V \rho(c_1, c_2, ...c_N)\, dV = 0 \tag{14}$$

However this model suffers from a major practical limitation; to produce a convergent numerical solution it is virtually required to assume global solution electroneutrality, which directly contradicts the purpose of this report. Therefore another model is needed which deviates from the Nernst Planck equations and where electroneutrality does not have to be assumed and a charge build up thus is possible.

The computability problems stem from the electrostatic feedback term describing how the ion distribution creates a potential field of its own, which is usually remedied by assuming charge neutrality. The practical alternative to assuming electroneutrality is neglecting the self-interaction term and working with the reduced equations. This reduced form of the Nernst-Planck equations is implemented in COMSOL under the "Transport of dilute species" which assumes that the ion interaction behaviour is that of an infinitely dilute solution. This workaround gives a workable model at the price of overestimating the ion accumulation.

Lastly the relation between the space charge density and the electric field is given by the Poisson equation:

$$\nabla \cdot E = \frac{\rho}{\epsilon_0} \tag{15}$$

wherein the space charge density is given from the ion concentrations according to equation 13.

4.4 The conductivity of a pure solution

An understanding of how ion concentration determines conductivity in a pure water solution is a good starting point for an understanding of the analog problem in tissue. This problem is an intricate topic in and of itself; not only is the conductivity of a single ionic species usually non-linear with respect to concentration, there are also many species in solution in the tissue. This non-linear behaviour is undesirable for modelling reasons, and the equations cannot be written on matrix form which hinders computability. However given that the separation of ionic species resulting from the electric field will be small compared to the overall concentration it is reasonable to linearize the model.

The linear conductivity model is thus formulated as first order polynomial expansion around the initial concentration point $\boldsymbol{c^{(0)}}$.

$$\sigma(\boldsymbol{c}) = \sigma_0 + \sum_{k=1}^{N} \frac{\partial \sigma}{\partial c_k}\bigg|_{\boldsymbol{c}=\boldsymbol{c^{(0)}}} (c_k - c_k^{(0)}) \tag{16}$$

To compute the coefficient data for the linearized model the hydrochemical solver Aqion was used. The program uses a diffusion coefficient and temperature based model [16] to calculate the conductivity at specified concentrations, and it was used to compute two data sets; 1: The total conductivity of a water solution with the same ionic concentrations as the extracellular fluid in the human body, and 2: Numerical derivative values for individual ion species at the aforementioned concentration.

For the sake of brevity let the vector containing all conductivity derivatives be:

$$\boldsymbol{\Gamma} = \frac{\partial \sigma}{\partial \boldsymbol{c}}\bigg|_{\boldsymbol{c}\,=\,\boldsymbol{c^{(0)}}} = \left[\frac{\partial \sigma}{\partial c_1}\Big|_{\boldsymbol{c}=\boldsymbol{c^{(0)}}} \quad \cdots \quad \frac{\partial \sigma}{\partial c_N}\Big|_{\boldsymbol{c}=\boldsymbol{c^{(0)}}} \right] \tag{17}$$

, the vectors containing the current and initial concentrations be:

$$\boldsymbol{c} = \begin{bmatrix} c_1 & ... & c_N \end{bmatrix} \tag{18}$$

and:

$$\boldsymbol{c^{(0)}} = \begin{bmatrix} c_1^{(0)} & ... & c_N^{(0)} \end{bmatrix} \tag{19}$$

respectively, and the bulk conductivity of the pure solution be σ_0. The linearized model for the conductivity of the pure solution can thus be written as:

$$\sigma(\boldsymbol{c}) = \sigma_0 + \boldsymbol{\Gamma}(\boldsymbol{c} - \boldsymbol{c^{(0)}})^T \tag{20}$$

Using AQION the values for σ_0 and Γ were then calculated. The value found for σ_0 was:

$$\sigma_0 = 2.1125\ \Omega^{-1}m \tag{21}$$

and the values in Γ were found to be:

$$\boldsymbol{\Gamma} = \begin{bmatrix} \Gamma_{Na} & \Gamma_K & \Gamma_{Ca} & \Gamma_{Cl} \end{bmatrix} = \begin{bmatrix} 5 & 7.4 & 8.2 & 7.8 \end{bmatrix} \Omega^{-1}m^2mol^{-1} \tag{22}$$

4.5 Conductivity and diffusion in tissue

The human forearm is an interspersed weave of solid tissue and fluid. It is the fluid that carries the ions that can form currents under an electric field, which is what allows for the conduction of electricity. However since the fluid is contained between fibers, membranes, and bone the movement of the ions is obstructed and the conductivity is less than in a pure solution. To model this complex phenomenon a semi-empirical diffusion model is here derived from data.

Material obstruction of ion movement

Beginning with the Nernst-Einstein equation for limiting molar conductivity for an ion species i [17]:

$$\Lambda_i^{(0)} = \frac{z_i^2 F^2}{RT} D_i \tag{23}$$

which relates the molar conductivity (conductivity per unit concentration) at infinite dilution to the diffusion coefficient D, ion charge z, Faradays constant F, gas constant R and the temperature T. This relation allows for the comparison between the diffusivity constants in pure solution and in tissue given the ratio of the two corresponding conductivities.

Let the reduced diffusivity for a single ionic species i in a certain tissue be related to the pure-solution diffusivity through the material factor $\alpha^{(i)}$:

$$\frac{D_{tissue}^{(i)}}{D_{solution}^{(i)}} = \frac{\Lambda_{tissue}^{(i)}}{\Lambda_{solution}^{(i)}} = \alpha_{tissue}^{(i)} \tag{24}$$

The diffusivity reduction coefficients for all ionic species could be calculated this way, but unfortunately there is not sufficient data on the individual conductivity contributions of different ions in human tissue to do this. Instead an assumptive condition can be imposed which grants that all ions have their diffusivities reduced by the same factor in a specific tissue type. This allows for the derivation of a general material constant α_n which governs both the reduction in diffusivity and conductivity for all ions in a given tissue type n.

Known tissue conductivites [3] along with the calculated pure-solution conductivity can then be used to derive the material constants for all tissue types. Using the values in table 1 for empirical tissue conductivities σ_e the α-values for the relevant tissue types can be derived, as shown in the table below:

Tissue	Skin	Fat	Muscle (axial)	Muscle (planar)
σ_e	0.0014285	0.03030	0.3333	0.1111
α_n	0.0006762	0.01434	0.1578	0.05260

Table 2: The experimentally measured conductivities of different tissues and their corresponding obstructivity constants.

Cortical bone and bone marrow was not included in the ion drift model because of the material's distance to the electrodes and their relative impermeability.

Diffusivity of obstructed ions

Each ion species has its own diffusivity constant D in water, which can readily be found in the literature for infinite dilution at 25C^o [18]. In order to find the diffusivity values in human tissue at 37C^o a few transformations and approximations have to be made.

First the result of the temperature dependence is modelled using the Stokes-Einstein approximation [19]:

$$\frac{D_{T_1}}{D_{T_2}} = \frac{T_1 \mu_{T_2}}{T_2 \mu_{T_1}} \tag{25}$$

where D is the diffusivity, T is the temperature, and μ is the dynamic viscosity of water at the given temperature. This allows for the approximation of the ion diffusivities in pure water at 37 C^o given the viscosities of water at the temperatures 25C^o and 37C^o which are found in the literature [20]. (It is assumed here that the viscosity of the extracellular fluid has the same relative temperature dependence as water).

Secondly the material obstructivity values are applied to yield the diffusivity for an ion species i in a given tissue n:

$$D_n^{(i)} = \alpha_n D^{(i)}\big|_{T=37^o} \tag{26}$$

4.6 Final conductivity model and parameters

All requirements have now been met to finalize the model and calculate all the necessary material parameters. The final conductivity model takes the form:

$$\sigma(\boldsymbol{c}, n) = \sigma_e^{(n)} + \alpha_n \Gamma (\boldsymbol{c} - \boldsymbol{c^{(0)}})^T \tag{27}$$

where $\sigma_e^{(n)}$ is the empirical conductivity for the tissue n.

These empirical conductivities are found below given in $\Omega^{-1}m^{-1}$ [3]:

Tissue	Skin	Fat	Muscle (axial)	Muscle (planar)
σ_e	0.0014285	0.03030	0.3333	0.1111

Table 3: The empirically determined conductivities for each tissue type in the ion model.

The calculated concentration conductivity derivatives in each tissue are given below in $\Omega^{-1}\text{m}^2\text{mol}^{-1}$:

Ion / Tissue	Skin	Fat	Muscle (axial)	Muscle (planar)
Na^+	0.00338	0.0717	0.789	0.262
K^+	0.0050	0.106	1.17	0.389
Ca^{2+}	0.0055	0.0118	1.29	0.431
Cl^-	0.00527	0.112	1.23	0.410

Table 4: Conductivity derivatives for each modelled ion type in each tissue type.

And finally the diffusivity constants for each ion and tissue are given below in 10^{-12} m^2/s:

Ion / Tissue	Skin	Fat	Muscle (axial)	Muscle (planar)
Na^+	1.20	25.44	279.8	93.31
K^+	1.76	37.33	410.7	136.9
Ca^{2+}	0.712	15.11	166.2	55.4
Cl^-	1.827	38.76	426.5	142.1

Table 5: Diffusivity constants for each ion type in each tissue type.

4.7 Cable Equation

While the Maxwell differential equations describe the electrial field well in the human tissue another model is needed in order to investigate when axons are activated. In the Kuhn thesis four models are presented, with one model displaying superior performance [3]. However as this report focuses on the relative impact of ionic effects as opposed to accurate nerve activation prediction this report uses the simplest model from the Kuhn article.

This section is based on the work of McNeal [21] in using the cable equation to a describe a myelinated axon. It can be described by the following equation:

$$\tau_m \frac{\partial V_{TP}}{\partial t} - \lambda^2 \frac{\partial^2 V_{TP}}{\partial x^2} + V_{TP} = \lambda^2 \frac{\partial^2 V_e}{\partial x^2} \tag{28}$$

where λ is a space constant, τ_m membrane time constant, V_{TP} is the threshold potential and V_e the extracellular potential [3]. An equivalent circuit from this equation can be seen below.

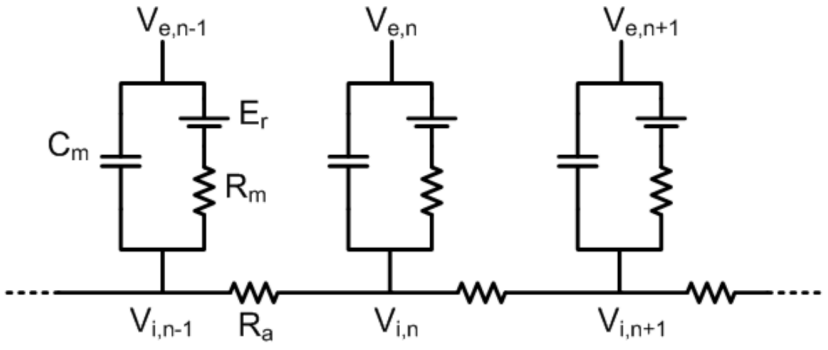

Figure 6: An equivalent circuit for a myelinated axon based on McNeals work [3] (Non-Commercial use permitted).

The right side term in equation 28 has been showed to be the driving force of the activation of an axon [22]. The Rattay article coined the phrase activation function for the second derivative, whereupon Kuhn's article examined different threshold potentials for the activation function. These are given in the table below.

AF^{th}		Pulse Duration [msec]					
		0.1	0.2	0.3	0.5	1	2
Axon $\varnothing$ $[\mu m]$	4	36178	20424	15086	10836	7733	6212
	6	12388	6888	5048	3596	2558	2084
	8	5328	2973	2188	1573	1143	964
	10	3010	1674	1230	882	643	553
	12	2117	1177	864	619	453	394
	14	1588	881	646	462	336	294
	16	1190	661	484	347	254	223

Figure 7: Thresholds calculated by [3] from the model created by Rattay [22] (Non-Commercial use permitted).

5 Limitations and implementation

This section serves to discuss the limitations of the developed model and how the implementation in COMSOL was made.

5.1 Model limitations and their implications

As mentioned previously a few significant concessions had to be made to obtain a computable model. Mainly the electrostatic ion-ion interactions had to be neglected in order to couple the systems of electrical currents and ionic flow. (In practical terms this is because COMSOL does not allow for the coupling of the equations for electric currents with the equations for ion behaviour.) As the ion self-interaction causes repulsion in the ion accumulation layer this neglection will inevitably give rise to a systematic overestimation of ion concentrations.

It is however possible to simulate electrically induced ionic drift with ion self-interaction under the condition that there are no electrical currents (i.e. through pure electrostatics). By comparing the results from coupled and non-coupled electrostatic simulations the degree of overestimation produced by the reduced model can thus be estimated and accounted for.

These comparative simulations are carried out later in chapter 10.

5.2 Implementation

This project relies on one key asset for computation: COMSOL. The first task is to create a geometry based on the Kuhn article with some augmentations for ease of use.

Geometry and mesh

In Kuhn article a forearm was created by parameters given in table 1, however as the problem in this report always can be seen as axis symmetric only half of the geometry was created with symmetry conditions on the boundary. Moreover only the upper part of the arm is of interest in almost all cases, and thus the geometry resolution was sectioned to prioritize this

area. A detailed guide for implementing this geometry and mesh can be found in appendix section 12.1.

Implementation of conductivity model

There are two principal study cases constructed in COMSOL for this work. The first one uses the previously described arm geometry along with the equations for electric current and transport of diluted species. However the latter required very special care and diligence and will thus be covered later in section 10. A detailed step-by-step-guide to implement the first model can be found in appendix section 12.2.

Parametric sweeps and waveform studies

Parametric sweeps (i.e. parameter space exploration through sequential simulations) were utilized to gather data on the effect on ion drift and input waveform. The first simulation series studied how changing the ion charges from 0-100% of their actual charges affected the simulation results. This was done by parametrizing the ion charge values in the "Transport of dilute species" tab to multiples of the variable "c_ion" (i.e. sodium having a charge of +c_ion and chloride -c_ion etc). A parameter sweep of c_ion was then made for values from 0 to 1, with a J_{in} value of 16 A/m^2.

Secondly the current waveform input was studied by using different time-dependent input currents rather than a constant value. Two waveforms of interest were chosen alongside the step function; A decreasing exponential function and a sinusoidal bell. These functions were amplitude normalized such that the total transmitted charge was the same. For the nominal constant current a 10 mA current was used for 5 ms, or 16 A/m^2. The total equivalent charge transmitted is thus 16*0.005 = 0.08 A*s/m^2.

The first function is defined as:

$$f(t) = 65 * e^{-800t} \tag{29}$$

$$\int_0^{0.005} f(t)dt = 0.0797619 \tag{30}$$

And the second function is defined by:

$$g(t) = 25.2 * sin(630 * t) \tag{31}$$

$$\int_0^{0.005} g(t)dt = 0.0799986 \tag{32}$$

The second spatial derivative of the potential distribution was then computed.

The shape of the three waveforms used in this study is plotted below. Note that the amplitude is normalized to one in the function implementation and is amplitude corrected during the simulations.

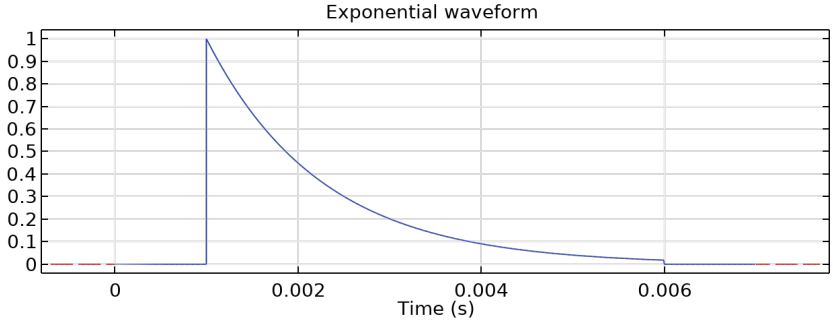

Figure 8: Waveform shape of the exponential wave used in the waveform study.

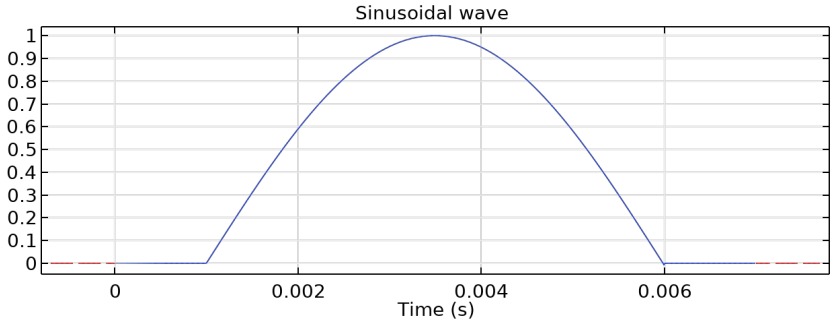

Figure 9: Waveform shape of the sine wave used in the waveform study.

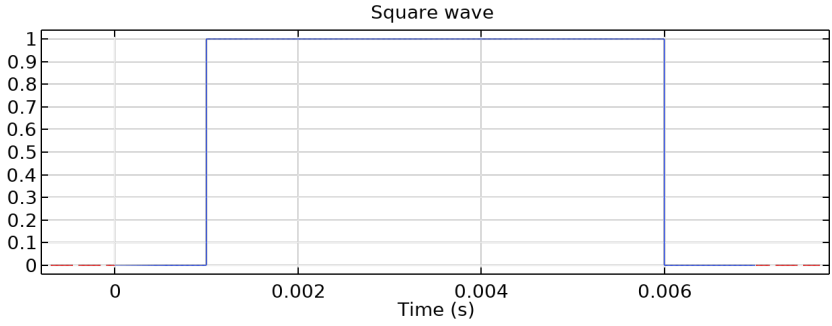

Figure 10: Waveform shape of the standard square wave used in the waveform study as well as in the conductivity model studies.

Note that the square wave is the standard waveform used in the other simulations in this report.

6 Results

6.1 Conductivity

First out the augmented conductivity model was studied. To this end a simulation was run with an input current of 10 mA for 5 ms, with the relative tolerance (solver error tolerance in relation to solution magnitude)

set to 10^{-4}, a time step size of 0.333 ms and the high resolution mesh. Four different data sets from the solution were studied; The electric potential and its second spatial derivative along the cut lines in figure 11, as well as the charge accumulation distribution and the integral of the accumulated charge in a specified control volume.

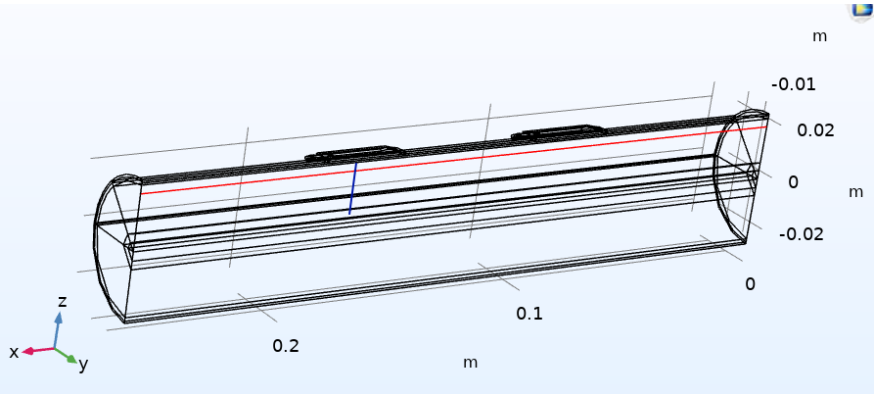

Figure 11: Horizontal red cut line along x = 0 to x = 1 , y = 0 and z = 0.02, as well as vertical blue cut line along x = 0.1725, y = 0, and z = 0.008 to z = 0.02425.

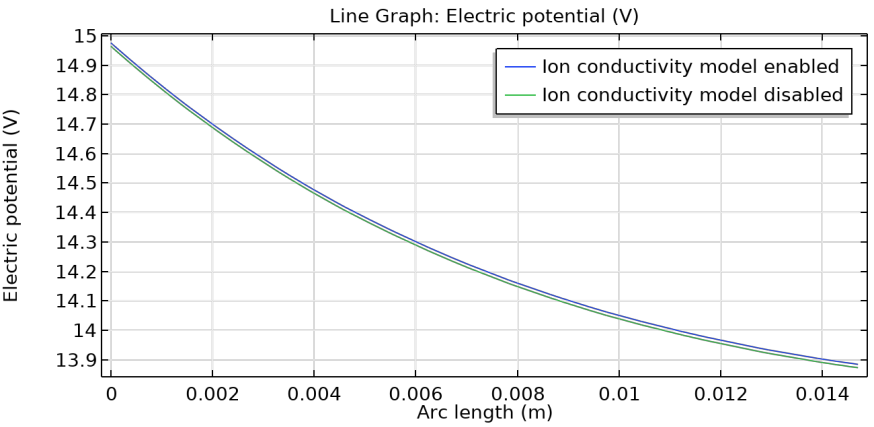

Figure 12: Two voltage graphs for the blue cut line given in figure 11. The upper graph represents voltage as when conductivity is included in the model and the lower graph for when conductivity is not included. Graph is taken after a complete run of 5 ms.

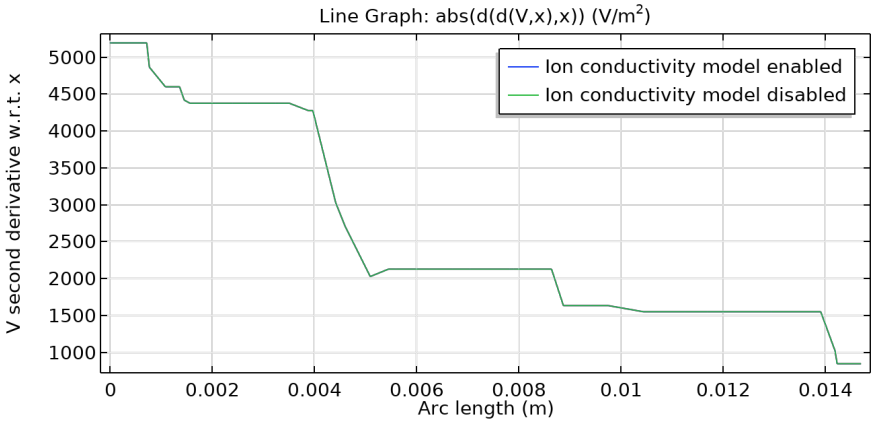

Figure 13: Two graphs for second derivative w.r.t x for the blue cut line given in figure 11. Note derivative w.r.t x due to nerves assumed to be running in x direction only. The two lines represent with/without conductivity model; the two cannot be distinguished here. Graph is taken after a complete run of 5 ms.

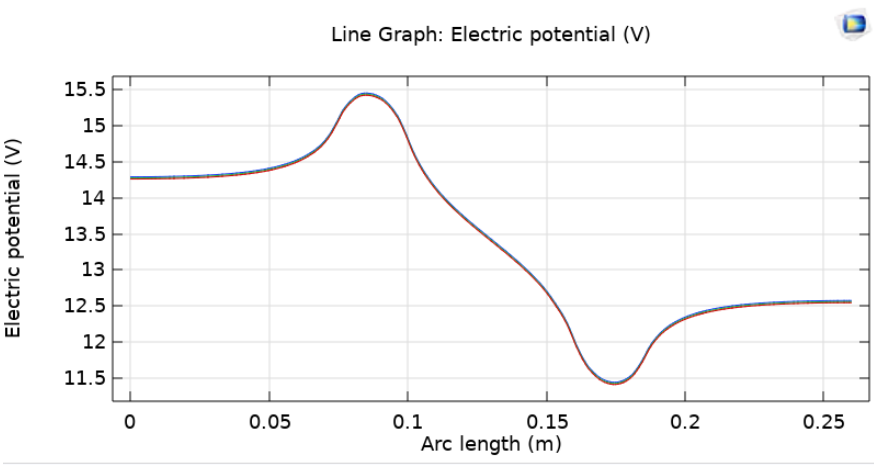

Figure 14: Two voltage graphs for cut line give in figure 11. The upper graph represents voltage as when conductivity is included in the model and the lower graph for when conductivity is not included. Graph is taken after a complete run of 5 ms. Note average voltage of ~13 V in the arm due to electrode contact resistance.

The charge density accumulation in C/m^3 is depicted in the figure below.

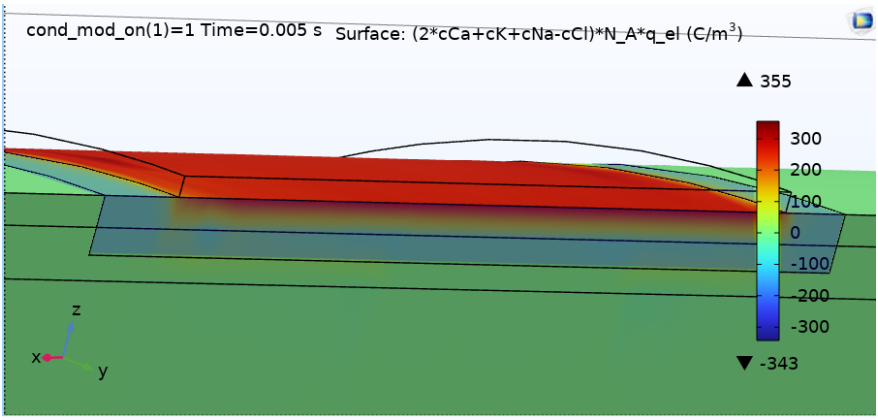

Figure 15: Charge accumulation with conductivity model. Control volume for integration is marked in blue.

The integral of total charge density in the immediate vicinity of the positive electrode is -3.3851E-4 [C]. (The result for the ground electrode is 3.3901E-4 [C] which means symmetry is preserved and that the numerics are sound). A closer look of the control volume for the charge accumulation can be seen above in the volume marked with blue.

Streamlines for the flux of the different ionic species were then studied to gauge the physicality of the results, and the results are depicted below.

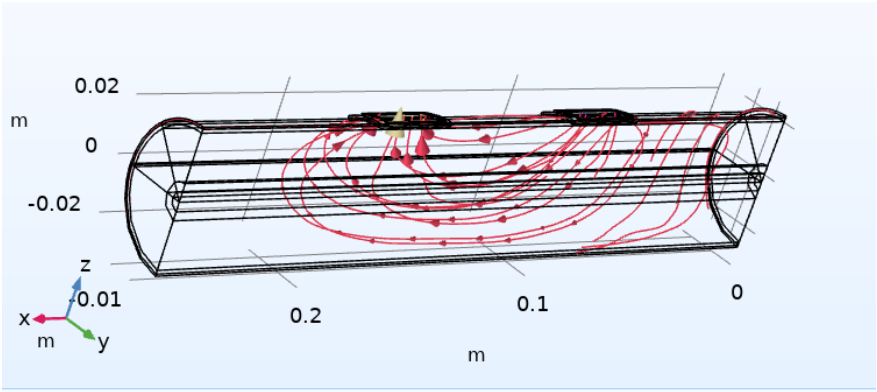

Figure 16: Streamline graph for calcium ion flux after 5 ms of 10 mA current flow

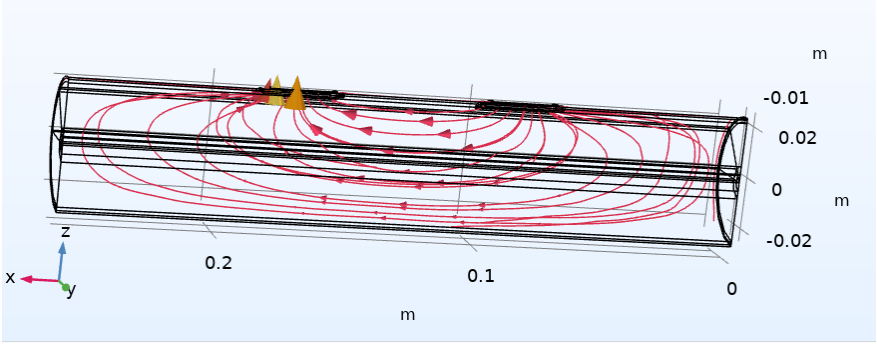

Figure 17: Streamline graph for potassium ion flux after 5 ms of 10 mA current flow

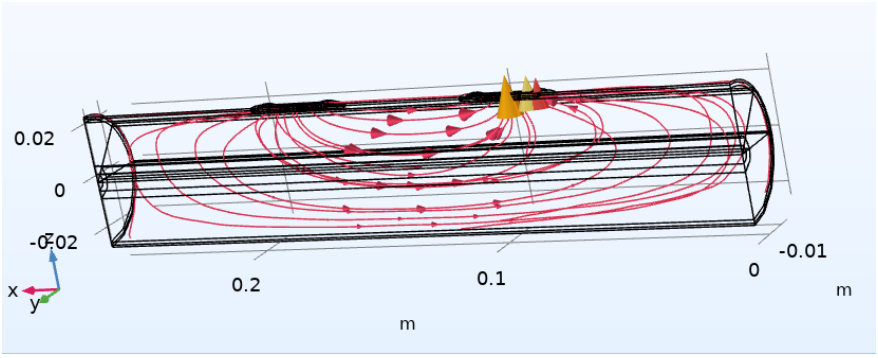

Figure 18: Streamline graph for chloride ion flux after 5 ms of 10 mA current flow

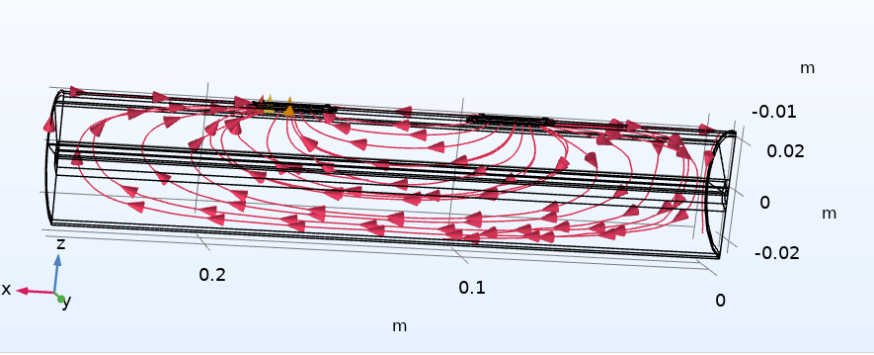

Figure 19: Streamline graph for sodium ion flux after 5 ms of 10 mA current flow

6.2 Waveform shape study

The second spatial derivatives for all wave forms and time steps are plotted below normalized for input current. The figure is plotted on the blue cut line given in figure 11.

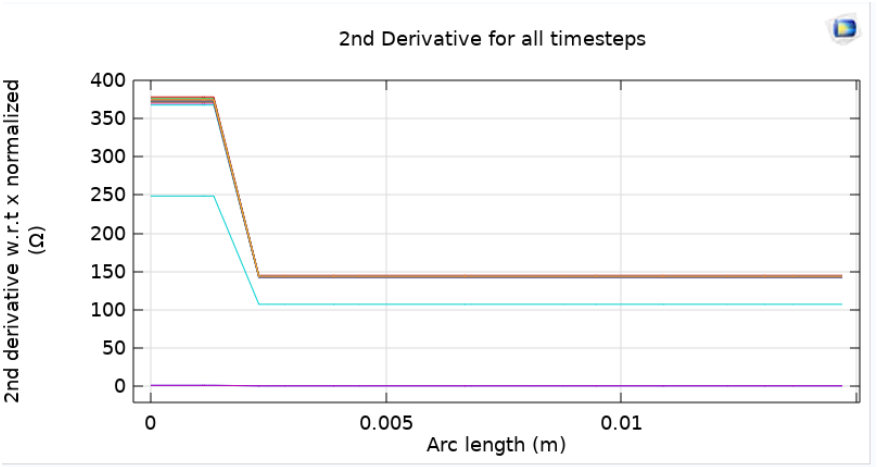

Figure 20: Second derivative w.r.t x for the three different runs with normalized data according to input. Plotted is the normalized second derivative for all three runs for all time steps. The reason for turquoise line not being 0 or identical to the others is that it represents the last time step before the sinusoidal wave reaches 0, and is rounded erroneously due to floating point errors. This is reasonable as it is then almost zero. Graphs taken from blue line in graph 11

7 Verification of model

A major part of implementing a FEM model is to complete verification studies in order to argue that the derived results are correct. In this report we have completed five verifications; The model is not dependent on time step size, the model produces similar results when altering the relative tolerance, the output current and input current in the electrodes are approximately the same, and the model asymptotically approaches the conventional volume conductor model as the ion charge approaches 0.

7.1 Verification of boundary condition validity

In COMSOL after a run it is possible to integrate the output current density as well as the input current density by creating a surface integral under derived values with the expression:

$$nx * ec.Jx + ny * ec.Jy + nz * ec.Jz \tag{33}$$

For a test simulation with an input current of 5 mA the intput integral was result 5.0001 mA and the input output integral was 4.9863 mA, when running with the relative tolerance 1e-7.

7.2 Dependence on time step size

When completing a FEM model it is of importance that results do not vary drastically while changing time steps. In this section the normal run is completed with time steps 1e-5, 5e-4, 1e-4, 1e-3 s and relative tolerance 1e-3.

A cut line was created at the z coordinate 0.0225 m and through the entire cylinder where the voltage was observed for different time steps. This gave the graph below which points towards the model not to be heavily affected by stepsize.

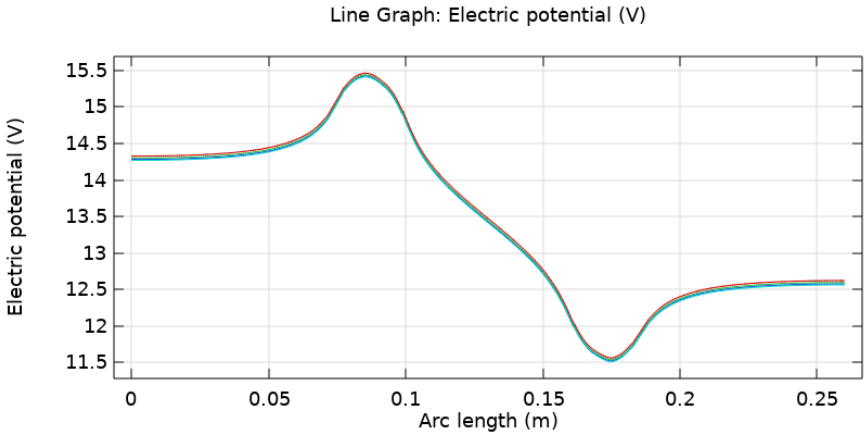

Figure 21: Time step verification graph. Graphs for time steps 1e-5, 5e-4, 1e-4 an 1e-3 s taken after 5 ms.

7.3 Altering of relative tolerance

Two simulations were made with relative tolerances 1e-3 and 1e-6. The results are depicted below.

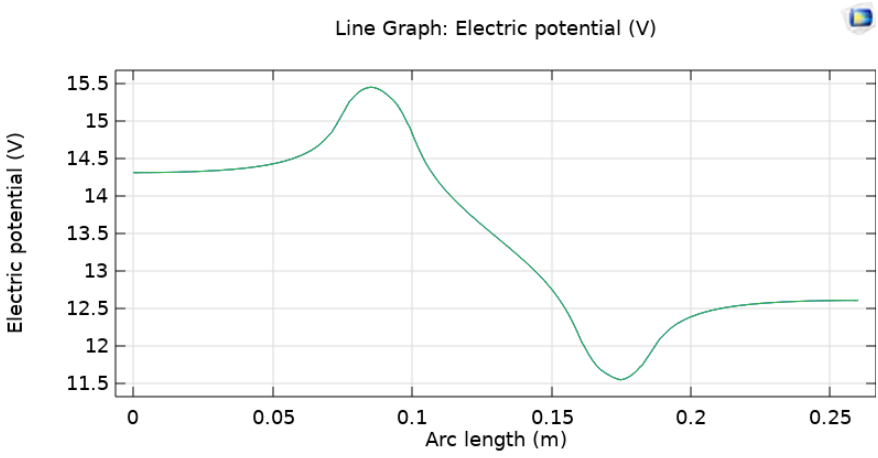

Figure 22: Verification of relative tolerance. Graphs taken for 1e-3 and 1e-6 relative tolerance. Graphs taken after 5 ms.

The two results are so similar that they appear as one line in the graph.

7.4 Dependence on ion charge

Another verification step is letting the charge of the ions depend on a parameter "charge" which can be gradually reduced from 1 to 0 in order to study the model's behaviour in the limit. A cut line is created along the x-axis with y = 0 and z = 0.0255. The figures hereunder showcase the results:

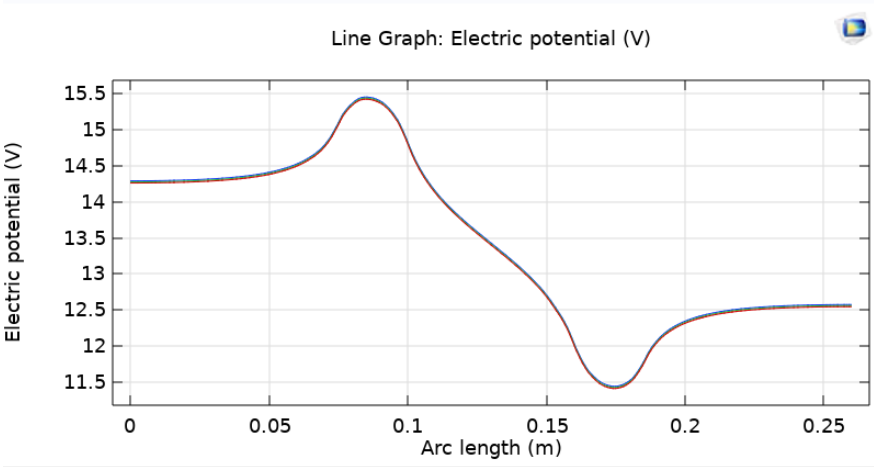

Figure 23: Three different graphs for charge = 1, 0.5 and 0. Where blue = 1, green = 0.5 and red = 0. Graphs taken after 5 ms.

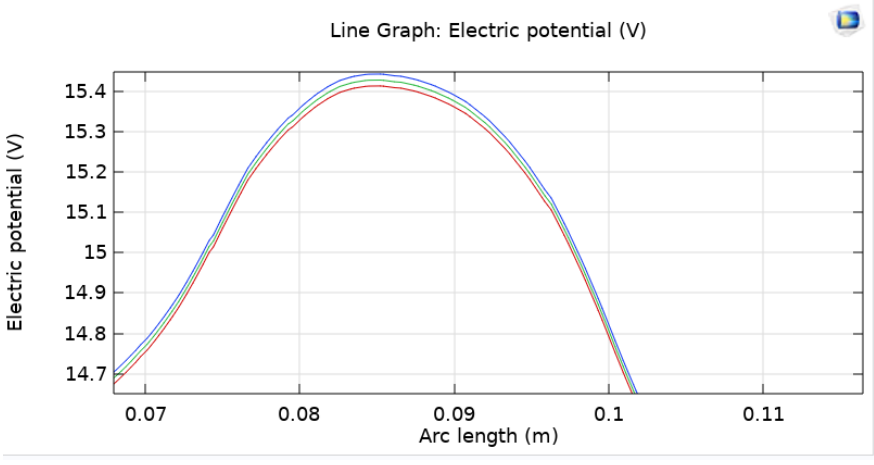

Figure 24: Three different graphs for charge = 1, 0.5 and 0. Where blue = 1, green = 0.5 and red = 0. Graphs taken after 5 ms. Zoomed in compared to upper figure

This occurs for the run with the conductivity model where an increased amount of ions give a decreased conductivity and thus increased voltage,

although the effects are very small. The plot below shows the change in conductivity stemming from the change in ion concentration:

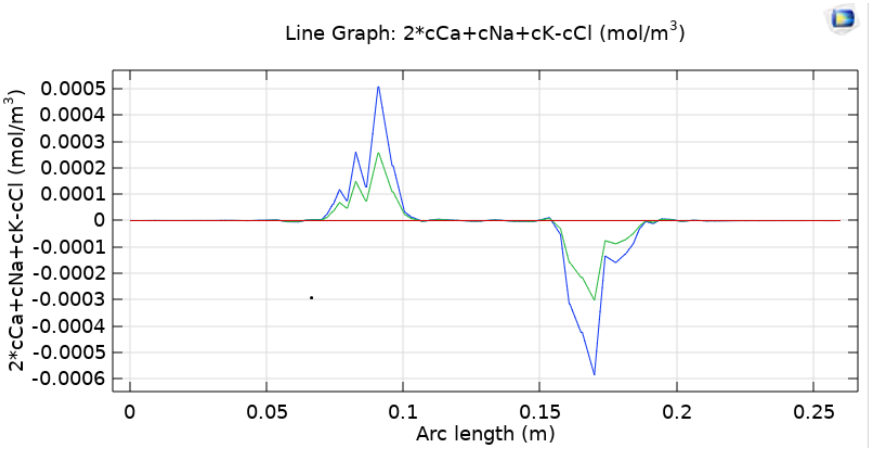

Figure 25: Differences in charge across a cut line along x-axis with y = 0 and z = 0.0255- Graph taken after 5 ms.

7.5 Dependence on mesh size

The same run was made with two different meshes in order to validate that they give approximately the same answer. The first one is run with "The good mesh" while the other is run with a mesh one degree more refined in all domains (i.e. "fine" instead of "normal" and "finer" instead of "fine" etc).

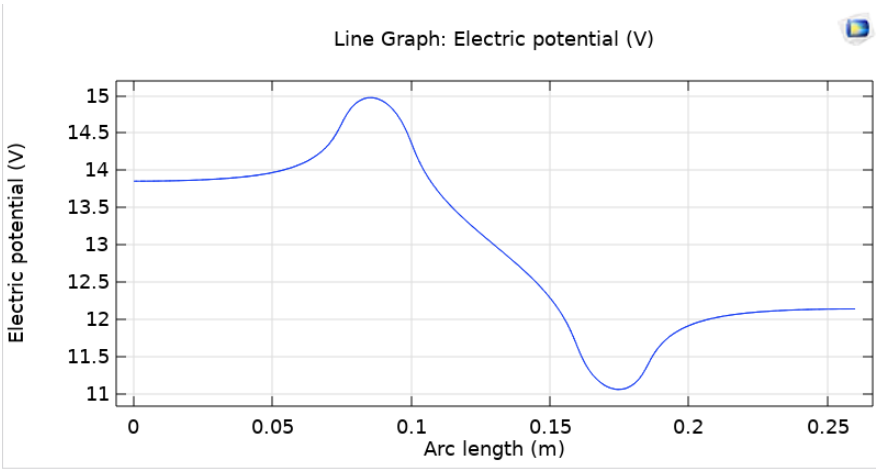

Figure 26: Good mesh

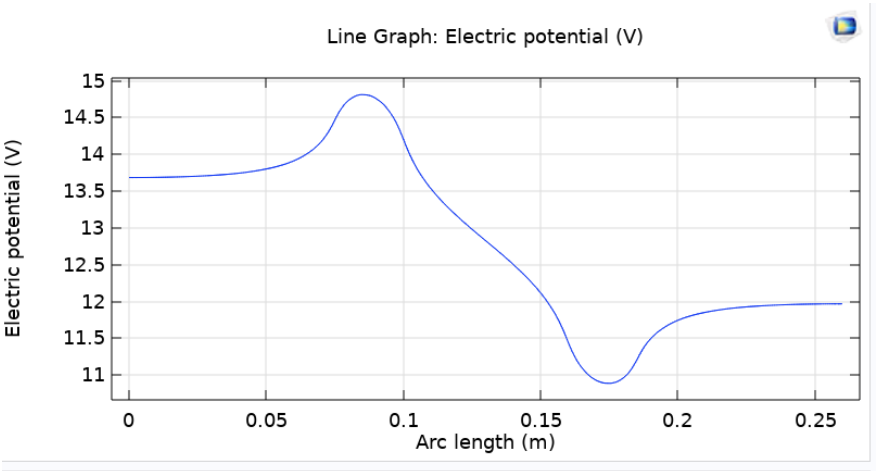

Figure 27: Voltage graphs for a cut line along x-axis with z = 0.0225 and y = 0. A small difference can be see in the peaks 14.81 V for the good mesh and 14.97 for the very good mesh- Graphs taken after 5 ms.

This showcases that mesh selection matters, however there is only a 1 % difference when it comes to the peak voltage. Although this makes clear the

importance of running the same mesh when comparing different models, the overall performance can be said to be mesh invariant.

7.6 Electrostatic control

In order to perform a reality check on the simulations above a brief analysis of the charge accumulation was made. The charge accumulated in the control volume during the transient simulation was integrated and used to calculate an average space charge density. This charge density was used to set up an electrostatic simulation to investigate the electric field generated from the accumulated ions.

Calculating the screening field from the accumulated ions will serve as a gauge of the overestimation; the real screening field is always smaller than the field from the electrodes. An overestimation was expected here since ion self-repulsion is a significant effect that is ignored, but the degree of overestimation is of interest. Thus the electrostatic simulation was setup with a space charge density of positive and negative 603 C/m^3 in the control volumes, and the resulting field can be viewed in the figure below:

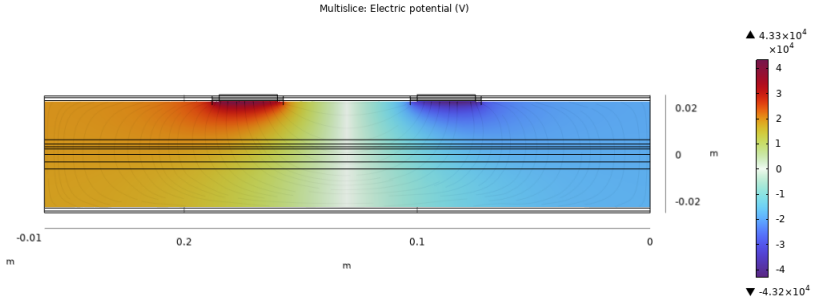

Figure 28: The potential given by charge accumulation from conductivity model.

This shows a very large degree of overestimation with a generated electric potential of tens of thousands of volts, indicating that the ion accumulation in the transient simulation is at least an order of magnitude too large. The fact that this overestimation is so large necessitates a further investigation using the full Nernst-Planck-Poisson equations.

During the simulations up to this point the total amount of accumulated ions has not depended significantly on mesh size, and because of this the comparative verification simulations have shown no mesh dependence on the potential field distribution. However the ion accumulation depth under the electrode has shown a strong mesh size dependence; it is typically constrained by the element size under the electrode. In order to fully rule out that the accumulated charge magnitude is mesh-dependent the mesh need to be refined to the point that the charge accumulation depth becomes independent from the mesh size. Thus a simulation using the full Nernst-Planck-Poisson equations and a very fine mesh

7.7 Overestimation due to neglect of electrostatic self repulsion and mesh resolution

When the assumption allowing for charge separation was made the electrostatic self-repulsion of the ions was neglected on the ground of computability. For the sake of computability it was also assumed that the mesh resolution was sufficient to arrive at a meaningful result. This section serves to explore the consequences of these assumptions by invoking the full Nernst-Planck-Poisson equations and by increasing the spatial resolution by many orders of magnitude.

The full Nernst-Planck-Poisson (NPP) model is much more computationally taxing than the nominal model and can only evaluate electrostatic problems. Therefore a new cylindrical test geometry was constructed in axissymmetric 2D to increase mesh resolution significantly, and the material was chosen to be isotropic with $\epsilon_r = 10^4$. The solution was set to have two ionic species with one positive and negative charge respectively and their diffusivities were chosen to be a constant 10^{-10} m^2s^{-1}.

The cylinder geometry has equal diameter and height, and on the inner half radius of the cylinder ends the boundary conditions of electric potential and ground are set. See example geometry below.

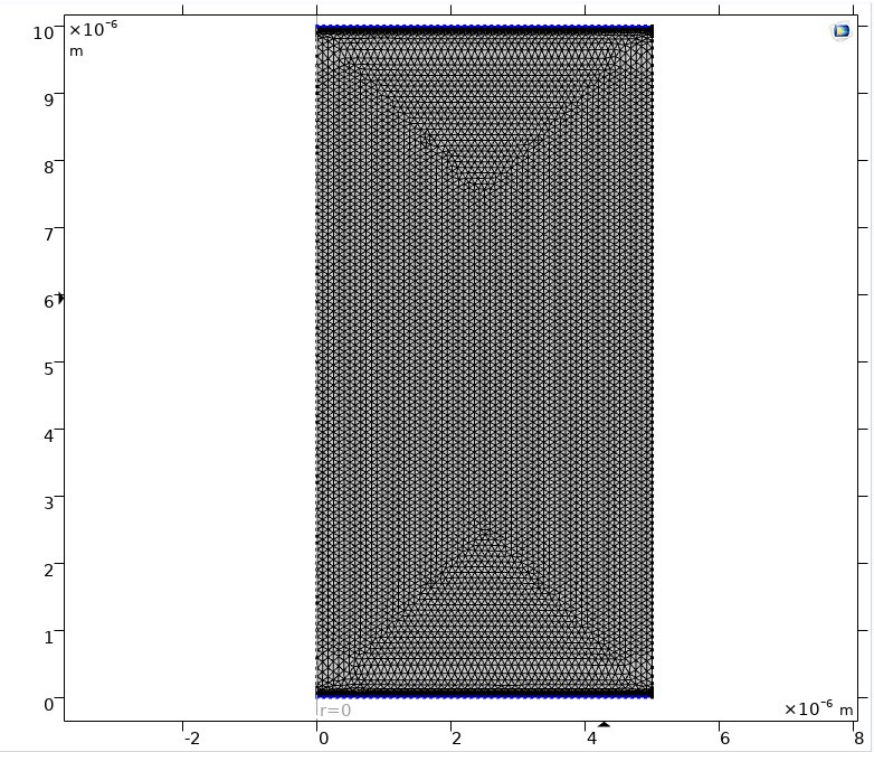

Figure 29: Example axissymmetric geometry mesh. Note the exponentially decreasing element size at the boundaries.

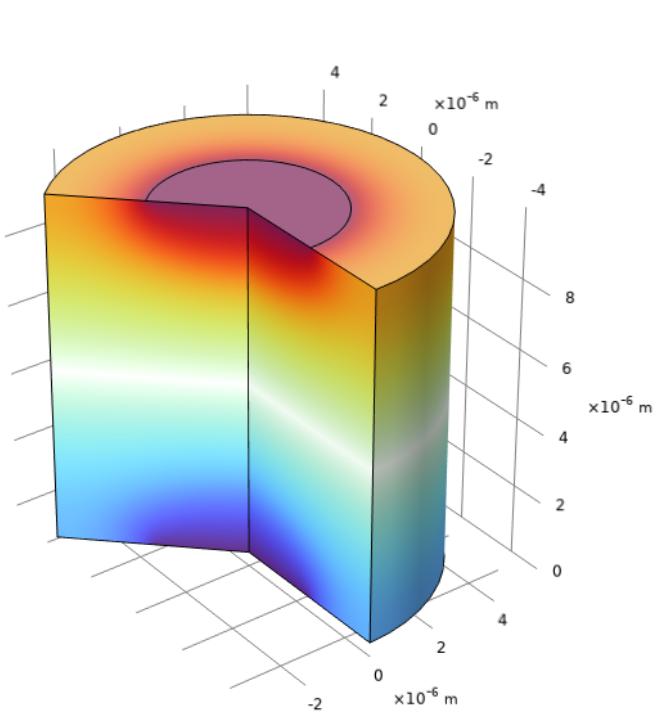

Figure 30: Example axissymmetric geometry with example potential distribution. Note boundary potential at bottom and top discs.

The ground electrode was set to 0 V and the positive electrode was set to a voltage that would yield 50 V/m between the two electrodes (i.e. 5 V if the cylinder is 10 cm high, 0.5 V if it is 1 cm high etc) in order to maintain a constant field strength and distribution with varying geometry size.

First the role of element size was investigated on the NPP equations. It was found that reducing the geometry and mesh size from a height of 10 cm and a boundary element size of 1 μm reduced the size of the ion buildup at the electrode in the solution. This indicated that the mesh size was too large for a physically accurate solution. It should be noted however that the total charge density accumulation did not change much with decreasing mesh size, indicating that only the accumulation layer thickness was obscured by

the mesh size variance.

Iterative reduction of geometry and mesh size was then made until a reduction of mesh size did not change the solution. Shown below is the sampling line on which the charge accumulations were evaluated.

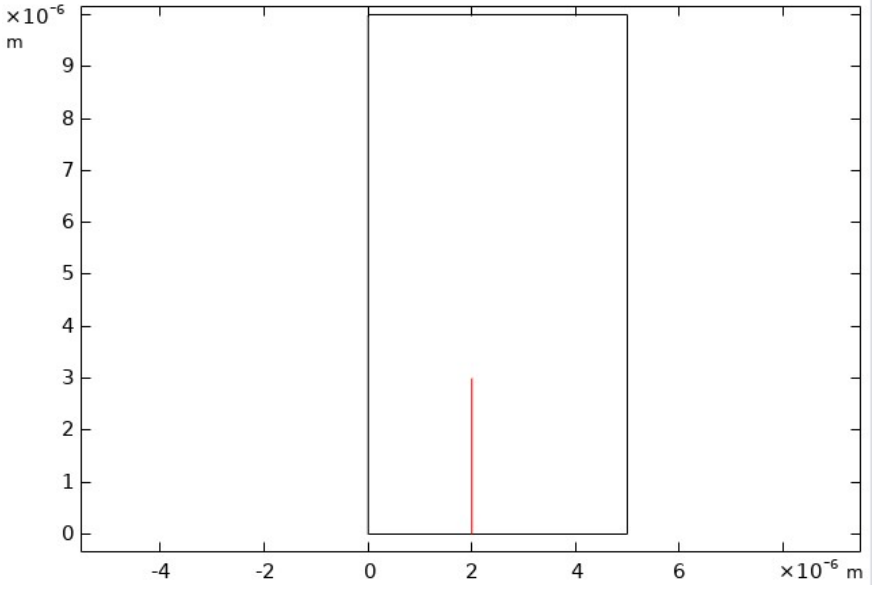

Figure 31: Sampling line for evaluating charge density close to electrode. The sampling line is at r = 2 μm, and ground boundary condition extends to r = 2.5 μm.

Total mesh invariance with good resolution was achieved with a cylinder height of 10 μm and a boundary element thickness of 0.4 nm. Below is the solution on the sampling line.

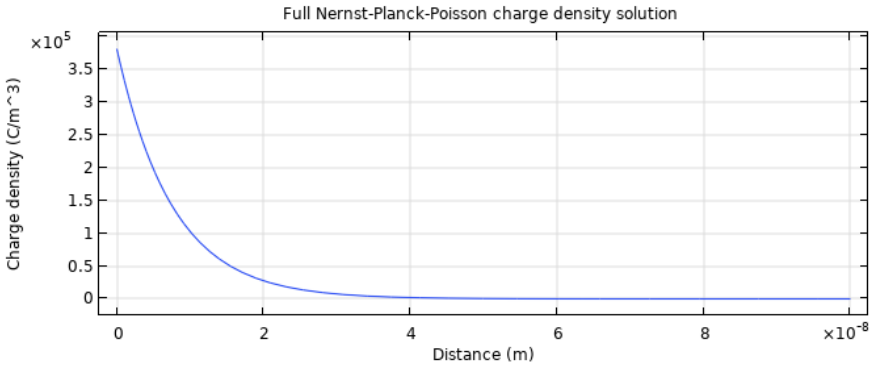

Figure 32: Nernst-Planck-Poisson solution close to electrode. Graph taken after 5 ms

With a sub-nanometer resolution it can be seen that the characteristic length of the ion accumulation layer is a few nanometers, while the total charge accumulation being comparable to that of the macroscopic mesh. This indicates that both the electrostatic screening and the change in resistance from ion concentration occurs much closer to the electrode than a macroscopic mesh would indicate. The corresponding voltage drop would thus also occur much closer to the electrode and further away from any nerves.

With the good model in hand the consequences of the electrostatic self-repulsion can be explored. This was done by disabling the multiphysics coupling between ion concentration and space charge density in the Nernst-Planck-Poisson physics module. This results in a model very similar to the original arm model, with no ion-ion interaction. The result can be seen below.

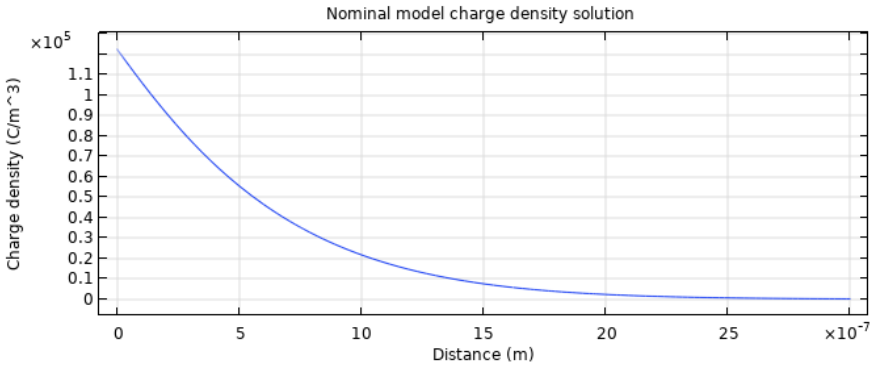

Figure 33: Solution without ion-ion interaction. Graph taken after 5 ms

Without the ion self-interaction the accumulation layer thickness is on the scale of micrometers instead of tens of nanometers, although the greatest peak charge density was found the NPP model. The total charge density integral along the sample line for the NPP model was:

$$\int_{\ell} \rho_{NPP}(l)\, \mathrm{d}l \; = 3.66 \cdot 10^{-8}\ \mathrm{C/m^2} \tag{34}$$

and the integral for the nominal model was:

$$\int_{\ell} \rho_{nom}(l)\, \mathrm{d}l \; = 8.99 \cdot 10^{-7}\ \mathrm{C/m^2} \tag{35}$$

The total ion accumulation was roughly 25 times greater in the nominal model compared to the full NPP model, and the accumulation layer was approximately 8 times thicker. The implications of this are twofold: Firstly the ion accumulation layer thickness calculated in the nominal arm model geometry is significantly overestimated due to the large mesh size, and secondly, the total concentration accumulation is most probably overestimated by an order of magnitude. It is however unclear why the ion accumula-

tion becomes more tightly concentrated towards the electrode when the self-repulsion is included. Because the charge magnitude and not the form factor is of interest here this phenomenon is not further investigated.

Overall this strongly suggests that the concentration- and charge accumulation-based changes in the electric field are overestimated in the nominal arm model.

8 Discussion

In this section the problem formulation questions will be answered, the results of the simulations will all be analyzed and the overall impact of this work will be commented on.

Regarding the first question, "is it possible to augment the existing TES model for predicting nerve activation with ion diffusion and drift" the answer is yes, with a few caveats. With the conductivity model we see changes in both the voltage graph in figure 12 as well as the second derivative in figure 13, although the change is very small. To add to this the electrostatic simulations (figure 28) indicate that these changes are at least an order of magnitude smaller in reality due to ion electrostatic repulsion. Therefore the conclusion of the original question is thus: It is possible to augment the existing model to obtain a more accurate model, however the increase in accuracy is negligibly small, and the implementation of the model would have to be done in a way that incorporates the electrostatic reduction in ion accumulation (which cannot be done easily in COMSOL). Moreover it increases the computational complexity substantially due to the introduction of new system equations and four new variables.

Lingering on this question, further conclusions can be drawn from the comparative axissymmetric Nernst-Planck simulations. In these simulations it was found that the boundary layer charge accumulation was incorrectly represented on a mesh with resolution comparable to the arm model, and that the true size of the layer did not become evident until the mesh size decreased below 1 nm. The discrepancies in both total charge accumulation and accumulation layer thickness due to modelling limitations was roughly one order of magnitude, implying that the results from the arm simulations

are off by a similar factor.

The impact of the resolution limitation on accumulation layer width is presumably small since the total charge buildup did not change with resolution, and because the charge accumulation layer was far away from any nerves even with a low resolution mesh. The impact of the overestimation of total charge accumulation is on the other hand probably significant, since both the screening effect and conductivity change in scale linearly with the total change in ion density. This suggests that the electrostatic self-repulsion should be a part of future models.

On the question of an eventual potential screening effect the answer is that it is most certainly negligible. The accumulated charge is small, and moreover it is localized in the boundary layer of the skin closest to the electrode. Thus any potential screening will be overridden by the constant-current boundary conditions, and any tissue below the boundary layer will not feel any difference. The same argument holds with concentration changes in the accumulation layer, since the change in conductivity from the ion concentrations occur far from any nerves of interest and will act more like additional electrode contact resistance.

Another question asked in the problem formulation is "Can the eventual effects of ion diffusion, be manipulated to alter nerve activation?". This was investigated by simulating three different wave forms and studying the normalized second derivative. The goal was to see if any differences in the activation-driving second derivative could explain the empirically observed effect that different stimuli shapes have on patient comfort. However as seen in figure 20 all functions and time steps (excluding 2 edges cases) have the same shape, leading to the conclusion that ionic effects as modelled in this work cannot account for the observed phenomenon.

The last question to be answered is "What is the next step in order to further mimic reality within this subject and which medically helpful inventions could it lead to?". A first step is that to recognize that this report has not been able to create a fully functional model that covers all relevant physics. This merits further investigation into questions such as "Can COMSOL or similar FEM software be used to correctly couple electric currents, ion space charge density, and ionic electromigration?". Developing a complete model

is quite a cumbersome task and would require a mathematical formulation that most likely would have to be implemented in the FEM software with custom code. In Glyn F. Kennel's doctor thesis he creates a mathematical framework for all these interactions except the ion-ion interaction, which could be a good extension to try and implement [23].

While this report limited itself to the use of the second derivative as an nerve activation function, one could use more accurate models (for example the MRG model [24] which the Kuhn thesis mentions to have the most reliable results [3]). It is also worth mentioning that ion flow can mechanically interact with cells, land closer to membrane channels and hence increase activation. This indicates that ion drift could be analyzed from different perspectives and scales in order to find other mechanisms which affect nerve activation.

9 Conclusion

The final conclusion to this report is that it is indeed possible to augment the conventional TES models with ion drift and diffusion, but that it is not practically useful. On top of this the augmented model cannot explain the importance of the current wave form, in fact it cannot even differentiate them based on the resulting potential distribution. Based on these findings it is thus not recommended to implement macroscopic ionic augmentations to the volume conductor model. Future research could perhaps focus on implementing more correct and rigid nerve activation models, or to implement ionic effect on the microscopic nerve-scale. An example would be to try and implement the mathematical framework from Kennels thesis [23] and to combine this with a model for how ions affect nerves on the scale of individual cells and axons.

References

[1] Jennifer Walinga and Charles Stangor. The neuron is the building block of the nervous system (creative commons attribution-noncommercial-sharealike 4.0 international license) https://creativecommons.org/licenses/by-nc-sa/4.0/. *Introduction to Psychology – 1st Canadian Edition*, 2014.

[2] Encyclopædia Britannica ImageQuest. Skeletal muscle structure, artwork [photograph]: https://quest.eb.com/search/132_1483015/1/132_1483015/cite.

[3] Andreas Kuhn. Modeling transcutaneous electrical stimulation. *ETH Zurich, Doctor Thesis*, pages 16, 17, 31, 34, 102, 103, 2008.

[4] Yvert Blaise Jouclai Sebastien, Gliere Alain. Current approaches to model extracellular electrical neural microstimulation. *frontiers in COMPUTATIONAL NEUROSCIENCE*, 2014.

[5] H. Saaroni J. Y. Lax, C. Price. On the spontaneous build-up of voltage between dissimilar metals under high relative humidity conditions. *Scientific reports*, pages 199–202, 2020.

[6] Milos R. Popovic Lazar I. Jovanovic, Martha G. Garcia-Garcia. Functional electrical stimulation pulse shape: Effect on comfort-related preference in individuals without neurological impairments. *Journal of Spinal Cord Medicine, The Volume 44, 2021*, 2021.

[7] Jonathan Laudanski-Katie E. Smith Daniel J. Jagger Daniel Gnansia Jimena Ballestero, Matthieu Recugnat and David McAlpine. Reducing current spread by use of a novel pulse shape for electrical stimulation of the auditory nerve. *Trends in Hearing, The Volume 19*, 2015.

[8] COMSOL. https://www.comsol.com/.

[9] COMSOL. Solutions to linear systems of equations: Direct and iterative solvers: https://www.comsol.com/blogs/solutions-linear-systems-equations-direct-iterative-solvers/.

[10] COMSOL. Solving nonlinear static finite element problems: https://www.comsol.com/blogs/solving-nonlinear-static-finite-element-problems/.

[11] COMSOL. Improving convergence of transient models: https://www.comsol.com/support/knowledgebase/1262.

[12] Physics Libre Texts. Time dependent maxwell's equations: https://phys.libretexts.org/Bookshelves/Electricity_and_Magnetism/Book$%$3A_Applications_of_Maxwells_Equations_(Cochran_and_Heinrich)/07$%$3A_Time_Dependent_Electromagnetic_Fields./7.02$%$3A_Time_Dependent_Maxwell$%$E2$%$80$%$99s_Equations.

[13] M. T. de Groot J. T. F. Keurentjes J. C. Schouten S. Moshtarikhah, N. A. W. Oppers and J. van der Schaaf. Nernst–planck modeling of multicomponent ion transport in a nafion membrane at high current density. *Journal of Applied Electrochemistry*, pages 51–62, 2017.

[14] Kazuhiko Seki Yohichi Suzuki. Solutions of the poisson–nernst–planck equations involving ionization for characterizing the influence of electrode reactions in a weak electrolyte. *Nanomaterials Research Institute(NMRI)*, 2017.

[15] COMSOL. Governing equations for the nernst–planck formulation: https://doc.comsol.com/5.6/doc/com.comsol.help.chem/chem_ug_chemsptrans.08.043.html#797637.

[16] Aqion. https://www.aqion.de/.

[17] Oxford. Nernst-einstein equation https://www.oxfordreference.com/view/10.1093/oi/authority.20110803100228898.

[18] Aqion. Table of diffusion coefficients https://www.aqion.de/site/diffusion-coefficients.

[19] Mandeep Dalal. Physical chemistry volume 1 - the stokes einstein relation https://www.dalalinstitute.com/wp-content/uploads/Books/A-Textbook-of-Physical-Chemistry-Volume-1/ATOPCV1-8-5-The-Stokes-Einstein-Relation.pdf.

[20] The Engineering Toolbox. https://www.engineeringtoolbox.com/water-dynamic-kinematic-viscosity-d_596.html.

[21] D. R. McNeal. Analysis of a model for excitation of myelinated nerve. *IEEE Trans Biomed Eng*, pages 329–337, 1976.

[22] F. Rattay. Modeling the excitation of fibers under surface electrodes. *IEEE Trans Biomed Eng*, pages 199–202, 1988.

[23] GLYN F. KENNELL. Electrolytic transport, electric fields, and the propensity for charge density in electrolytes. *University of Saskatchewan, Doctor Thesis*, 2011.

[24] A. G. Richardson C. C. McIntyre and W. M. Grill. Modeling the excitability of mammalian nerve fibers: influence of afterpotentials on the recovery cycle. *Journal Neurophysiology*, pages 6, 42, 45, 56, 64, 2002.

10 Can ions drift in a electric field be modelled to impact nerves activation answer? A popular scientific summary

This report studies if it is possible to more accurately predict how nerves activate during electrical stimulation if the electrical effects of ions are included. This was accomplished by developing a new model for how ions change the way human tissue conducts electricity and by simulating these effects in computer models.

The nerves we have in the human body can be activated to cause muscle contractions. This normally happens when a nerve cell receives a signal from another nerve cell, however this can also be achieved by exposing the nerve to an electric current. A common technique for this is to attach electrodes to the skin and to carefully pass current between them until the desired muscle activates. Because the ions are charged they "wander" towards its opposite charge in an electric field. This means that if an electric field is sufficient strong it is possible to move around enough ions to change the electrical properties of the tissue, and thus change how electricity passes through the nerves.

This report attempts to model the effects ions have on nerve activation by taking into account and modelling two phenomena; Electrical conductivity and charge accumulation. Electrical conductivity is a measure of how easy an electric current passes through a material, and by changing the concentration of ions using the electric field it is possible to change this property. Charge accumulation is what happens when ions of similar charge "pool up" in the same area and create their own electric field, which interferes with the electric field from the electrodes. Both these effects were modelled mathematically and then simulated in numerical simulations.

Lastly it was studied if the ionic effects could help explain the observed phenomenon that differently shaped electric pulses produce different outcomes in experiments. It has been shown that different pulse shapes lead to different levels of comfort and muscle activation in patient, but conventional models of nerve activation cannot account for this fact.

Unfortunately it was found that these ionic mechanisms could not signifi-

cantly improve prediction accuracy or help explain the observed difference between different pulse shapes. This could be due to the modelling simplifications that were made, or it might be implying that ionic effects are irrelevant on the macroscopic scale.

11 APPENDIX

11.1 Implementation of geometry and mesh in COMSOL

This section serves as a detailed step-by-step guide to implement the geometry and mesh in COMSOL.

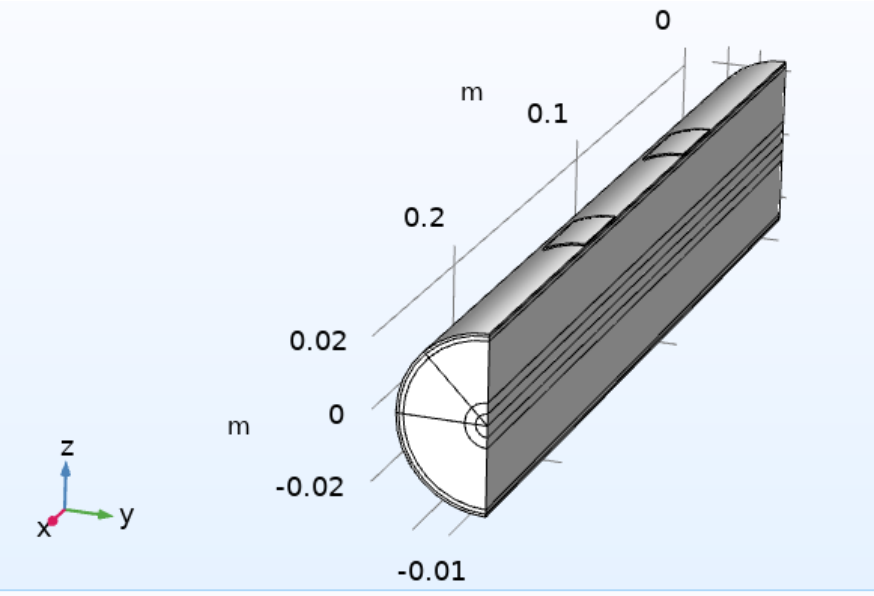

Figure 34: Geometry as built in COMSOL

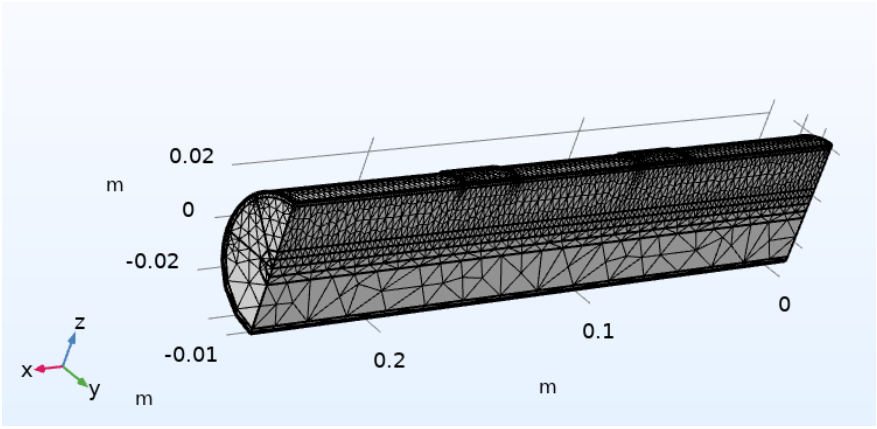

Figure 35: Meshed as built in COMSOL

The method used to create the geometry is detailed below:

- 1: Create 6 concentric cylinders with radii according to 1 and with a length of 26 cm.
- 2: Partition them using the boolean "Difference" operator such that no clipping occurs. This layered geometry will constitute the arm.
- 3: To create the electrodes first sketch their cross-section in a xy-workplane using circular arcs. Then extrude them to desired length and move them in the x-direction until desired spacing is attained.
- 4: To partition the geometry for prioritized resolution a cutting shape can be used. Make an extrusion of a 90^o circular arc with a radius greater than the arm's and with a length equal to that of the arm. Rotate the extrusion such that it overlaps with the desired volume in the arm, then use the "Partition volume" volume operator to segment the geometry into two parts.
- 5: If needed repeat this step to create more volumes for custom resolution. This was done twice in the used geometry as shown if figure 34.
- 6: To invoke bilateral symmetry one half of the geometry needs to be deleted. This can be done either by creating a block volume over-

lapping with half the arm and then using the "Difference operator", or by partitioning the arm using a xz-workplane and deleting one of the partitions. Do not forget to activate the symmetry nodes in the physics menu later.

- 7: Finish off the geometry by forming a union with "repair tolerance" set to "automatic"
- 8: Create two different meshes, one with high resolution ("The good mesh") as well as one with lower resolution ("The average mesh").
- 9: "The good mesh", set mesh resolution to "finer" in segmented high-res volume, "normal" on sides and "coarse" everywhere else.
- 10: "The average mesh": Set mesh resolution to "normal" in segmented high-res volume and "extra course" everywhere else

11.2 Implementation of conductivity model in COMSOL

This section serves as a step-by-step guide to implement the concentration-conductivity model in COMSOL.

- 1: Add Physics nodes "Electric Currents" and "Transport of Dilute species"
- 2: In the "Transport of dilute species" add 4 ion species variables (each for K^+, Na^+, Ca^{2+} and Cl^- respectively) and set up their initial concentrations according to table 36 in Appendix. Activate bilateral symmetry conditions, activate "migration in electric field", and then set the potential variable name to "V" to couple it to the "Electric currents" node. Do not forget to set the ion charges for the different ion species.
- 3: Under "Transport properties" in "Transport of dilute species" setup the diffusion coefficients as calculated in table 5.
- 4: In physics node "Electric currents" setup one electrode to be ground and another to have "Normal current density" with a variable value of "J_in". Activate bilateral symmetry conditions.
- 5: In the "Materials" node in the arm model manually define the

conductivites of the materials according to the linearized conductivity model by setting the values to function expressions.

- 5: Create a time-dependent study and choose the appropriate mesh.

11.3 Global parameter values

Below are the tables of global parameters used in the COMSOL implementation.

Name	Value
alphafat	0.014345
alphamx	0.15779
alphamp	0.05259697567
alphaskin	0.0006762468301
kNaskin	$0.0033812 s^3 \cdot A^2/(kg \cdot mol)$
kKskin	$0.0050042 s^3 \cdot A^2/(kg \cdot mol)$
kCaskin	$0.0055452 s^3 \cdot A^2/(kg \cdot mol)$
kClskin	$0.0052747 s^3 \cdot A^2/(kg \cdot mol)$
kNasfat	$0.071723 s^3 \cdot A^2/(kg \cdot mol)$
kKfat	$0.10615 s^3 \cdot A^2/(kg \cdot mol)$
kCafat	$0.11763 s^3 \cdot A^2/(kg \cdot mol)$
kClfat	$0.11189 s^3 \cdot A^2/(kg \cdot mol)$
kNamx	$0.78895 s^3 \cdot A^2/(kg \cdot mol)$
kKmx	$1.1677 s^3 \cdot A^2/(kg \cdot mol)$
kCamx	$1.2939 s^3 \cdot A^2/(kg \cdot mol)$
kClmx	$1.2308 s^3 \cdot A^2/(kg \cdot mol)$
kNamp	$0.26298 s^3 \cdot A^2/(kg \cdot mol)$
kKmp	$0.38922 s^3 \cdot A^2/(kg \cdot mol)$
kCamp	$0.4313 s^3 \cdot A^2/(kg \cdot mol)$
kClmp	$0.41026 s^3 \cdot A^2/(kg \cdot mol)$

Figure 36: Table of global parameter values.

sigmamp	$0.11111m$
sigmafat	$0.030303\Omega m$
sigmamx	$0.33333m$
c0Na	$150mol/m^3$
c0K	$3mol/m^3$
c0Ca	$1.4mol/m^3$
c0Cl	$155.8mol/m^3$
Jin	$16A/m^2$
dt	$0.3333ms$
tendsim	$5ms$
DNa	$1.7744E-9m^2/s$
DK	$2.603E-9m^2/s$
DCa	$1.0534E-9m^2/s$
DCl	$2.7028E-9m^2/s$
NA	$6.022E23mol^{-1}$
qel	$1.602E-19C$

Figure 37: More global parameter values.